Light Localization in Local Isomorphism Classes of Quasicrystals

Chaney Lin,[1*] Paul J. Steinhardt,[1,2] and Salvatore Torquato[1,2,3,4,5]
[1]Department of Physics, Princeton University, Princeton, New Jersey 08544, USA
[2]Princeton Center for Theoretical Science, Princeton University, Princeton, New Jersey 08544, USA
[3]Department of Chemistry, Princeton University, Princeton, New Jersey 08544, USA
[4]Program of Applied and Computational Mathematics, Princeton University, Princeton, New Jersey 08544, USA
[5]Princeton Institute for the Science and Technology of Materials, Princeton University, Princeton, New Jersey 08544, USA

(Received 12 November 2017; published 14 June 2018)

We study a continuum of photonic quasicrystal heterostructures derived from local isomorphism (LI) classes of pentagonal quasicrystal tilings. These tilings are obtained by direct projection from a five-dimensional hypercubic lattice. We demonstrate that, with the sole exception of the Penrose LI class, all other LI classes result in degenerate, effectively localized states, with precisely predictable and tunable properties (frequencies, frequency splittings, and densities). We show that localization and tunability are related to a mathematical property of the pattern known as "restorability," i.e., whether the tiling can be uniquely specified given only a set of rules that fix all allowed clusters smaller than some bound.

DOI: 10.1103/PhysRevLett.120.247401

The choice of orientational symmetry, quasiperiodicity, and the fundamental repeating units (e.g., tiles, atoms, molecules) does not uniquely specify a quasicrystal; there are infinitely many space-filling arrangements of the same repeating units, with the same symmetry and same support for their diffraction patterns [1–4]. See Fig. 1(a). They can be grouped into *local isomorphism* (LI) *classes*; two quasicrystals are in the same LI class if, and only if, any local configuration of the repeating units found in one can be found with the same frequency in the other.

This Letter investigates the photonic properties of pentagonal quasicrystal heterostructures across a continuous spectrum of LI classes composed of different arrangements of the same obtuse and acute rhombi. We demonstrate that these heterostructures, though defect-free, possess effectively localized states within their fundamental band gaps and that the frequencies, frequency splittings, spatial configuration, and concentration of the localized states can be precisely predicted and tuned *in advance* by varying the LI class or other parameters. This flexibility and control is advantageous in the design of optical cavities for use as radiation sources [5] or sensors [6]. Existing methods for generating localized states [7] through disorder (defects) have the challenge of identifying defect arrangements that minimize the interference between defects and, at the same time, enabling the ability to select the frequency splittings. At present, no such methodology exists for photonic quasicrystals. (For a review, see Ref. [8].)

We show that the existence and tunability of these states is related to the fact that, except for a countable subset of measure zero, the continuous spectrum of LI classes is *not restorable* [9,10]. A restorable tiling can be uniquely specified given only a set of rules that fix all allowed clusters smaller than some bound; a well-known example is the Penrose tiling [11], which satisfies J. Conway's "town theorem" [12], a specific type of restorability. Conversely, nonrestorable means that there exist local configurations of rhombi whose density can be made arbitrarily small by continuously scanning through the spectrum of LI classes. We find that it is these configurations that become the tunable localization sites.

Tilings and definitions.—The tilings are obtainable as direct projections from a five-dimensional hypercubic lattice or as duals to an overlapping set of five periodically spaced grids [13–15]. We use periodic approximants to compute the band structure and verify convergence with the level of approximant.

The approximants are generated using the "generalized dual method" described in Refs. [15,16], with one modification: instead of $\mathbf{r}_i = (\cos 2\pi i/5, \sin 2\pi i/5)$, the star vectors are chosen as follows:

$$\begin{aligned}
&\hat{\mathbf{r}}_0 = (1,0), \hat{\mathbf{r}}_1 = (\cos 2\pi/5, \sin 2\pi/5),\\
&\hat{\mathbf{r}}_2(n) = (-1, \tau_n^{-1}) \cdot (\hat{\mathbf{r}}_0, \hat{\mathbf{r}}_1),\\
&\hat{\mathbf{r}}_3(n) = -(\tau_n^{-1}, \tau_n^{-1}) \cdot (\hat{\mathbf{r}}_0, \hat{\mathbf{r}}_1),\\
&\hat{\mathbf{r}}_4(n) = (\tau_n^{-1}, -1) \cdot (\hat{\mathbf{r}}_0, \hat{\mathbf{r}}_1),
\end{aligned}$$

where $\tau_n = F_{n+1}/F_n$ $(= 1/1, 2/1, 3/2, 5/3, \ldots)$, and F_n is the nth Fibonacci number ($F_0 = F_1 = 1$). Examples from different LI classes are shown in Fig. 1(a). For the Penrose LI class, this procedure minimizes the density of defects—necessary to make the tilings periodic—to two mismatched edges per unit cell [17]. As $n \to \infty$, the approximants approach the ideal tiling; the number of vertices in the unit

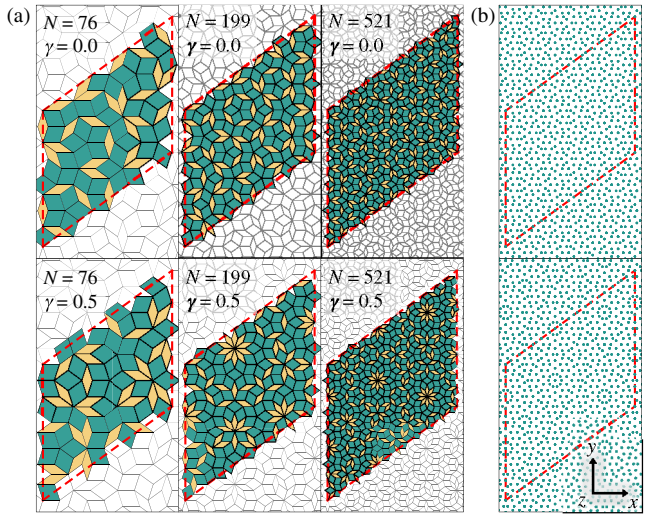

FIG. 1. (a) Examples of periodic approximants from two different LI classes (top to bottom) and from three different degrees of approximant (left to right). The LI classes are $\gamma = 0$ (top row) and $\gamma = 0.5$ (bottom row). The number of points in the unit cell for each approximant is $N = 76$ (left column), $N = 199$ (middle column), and $N = 521$ (right column). The unit cell for each approximant is outlined in dashed red lines. The tiles that form the unit cell are filled in, with obtuse tiles filled in with green and acute tiles filled in with yellow. (Some of the unit-cell tiles extend beyond the dashed red lines, because we have chosen here to completely fill in tiles (without repeats) that occur at the boundary of the unit cell, instead of truncating them.) (b) Example of dielectric structures derived from the $N = 521$ approximants in (a). Dielectric cylinders (filled in with green) have axes oriented along the z axis, which points out of the page.

cell increases; $\tau_n \to \tau = (1+\sqrt{5})/2 \approx 1.618$, the golden ratio; and $\hat{\mathbf{r}}_i(n) \to \mathbf{r}_i$, the star vectors of the ideal tiling. The tilings are composed of two types of rhombi, both with the same edge length a, but one with interior angle $2\pi/5$ ("obtuse") and the other with $2\pi/10$ ("acute"). In the limit $n \to \infty$, the ratio of the number of obtuse rhombi to the number of acute rhombi is equal to τ for all tilings; hence, in the $n \to \infty$ limit, all tilings have the same *number density*, i.e., the same number of vertices per unit area.

The displacement of the ith grid from the origin is the phase γ_i, and the sum of the phases $\gamma = \sum_{i=0}^{4} \gamma_i$ labels the LI class of the tiling. Two tilings are locally isomorphic (up to inversion) if, and only if, the sums of their phases $\gamma = \sum_{i=0}^{4} \gamma_i$, $\gamma' = \sum_{i=0}^{4} \gamma_i'$ are related by

$$\left| -\frac{1}{2} + \{\gamma\} \right| = \left| -\frac{1}{2} + \{\gamma'\} \right|, \tag{1}$$

where $\{\gamma\}$ denotes the fractional part of γ. The distinct values of γ lie within the interval [0, 0.5]; $\gamma = 0$ corresponds to the Penrose tiling. Any γ can be mapped to an equivalent one γ' within the interval [0, 0.5] via

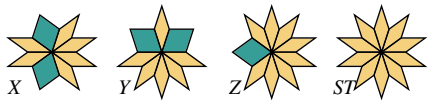

FIG. 2. The four special vertex environments.

$$\gamma' = \frac{1}{2} - \left| -\frac{1}{2} + \{\gamma\} \right|. \tag{2}$$

Moreover, if $\gamma, \gamma' \in [0, 0.5]$ and $\gamma \neq \gamma'$, then γ is not locally isomorphic to γ'.

A *vertex environment* is a configuration of tiles that shares a common vertex. There are 16 distinct vertex environments (up to rotation), and every LI class has a characteristic distribution of vertex environments (see Ref. [16] or [18]). The X, Y, Z, and ST vertices (using the notation of Refs. [13,14,19]) play an important role in our discussion. They are shown in Fig. 2, and we refer to them as *special vertex environments* (SVEs).

Setting up band structure calculation.—We compute the photonic band structure of dielectric heterostructures constructed by placing, on the tile vertices and oriented normal to the tiling plane, an array of parallel, infinitely long cylindrical rods with dielectric constant 11.56 (silicon) and radius $0.18a$ (filling fraction ~12.5%) in a background of air. The same radius (equivalently, the same filling fraction) is chosen for all structures to allow for fair comparison. Examples of such dielectric structures are shown in Fig. 1(b).

Maxwell's equations are solved for states with transverse magnetic (TM) polarization, i.e., with the electric field oriented parallel to the cylindrical axis [the z axis in Fig. 1(b)]. The TM band structure is calculated using a supercell approximation and the plane-wave expansion method [20,21]. Spatial resolution of the unit cell is chosen to be 512×512. For $N = 521$ approximants, the frequencies computed at this resolution differ by less than 0.1% of those computed at 1024×1024 resolution. We compute the lowest $1.1 \times N$ bands, which reliably contain the first sizeable band gap.

For quasicrystals, the photonic band gaps and the neighboring bands are known to be highly isotropic [22,23]. Therefore, we simplify our analysis by restricting our computation of spectra to the $\mathbf{\Gamma} = (0,0)$ and $\mathbf{M} = (\mathbf{b}, 0)$ symmetry points, where $\mathbf{b}$ is one of the basis vectors of the reciprocal lattice. These are defined for the hexagonal first Brillouin zone, corresponding to the rhombic unit cell of the approximant.

Results.—Whenever a SVE appears in a tiling, the TM band structure contains states in which the electric field is highly concentrated on the SVE, either on one isolated site or on many sites. Figure 3 shows representative examples of these states on isolated sites.

Take one of these states and let r be the radial distance from the central vertex. We observe that the energy density

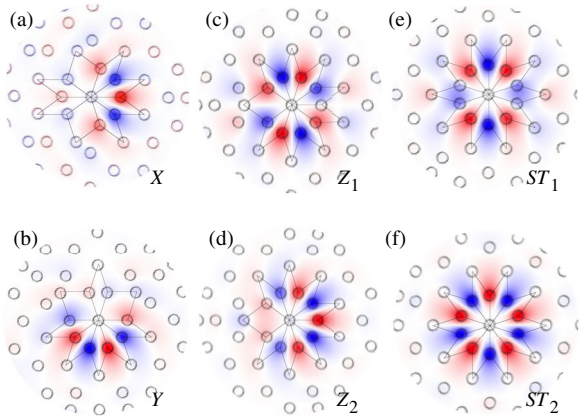

FIG. 3. Representative electric field distribution for the six observed types of effectively localized states. Blue, red, and white correspond to a minimum, maximum, and zero power for a given state, respectively. Contours of dielectric cylinders are shown, and the vertex environments are overlaid (see Fig. 2). (a) X, (b) Y, (c) Z_1, (d) Z_2, (e) ST_1, and (f) ST_2.

$u(r)$ (the square of the field) peaks around $r \approx a$—where the first nearest neighbors are located—then drops to $\lesssim 0.1\%$ of the peak by around $r \approx 2a$. The field thus appears to be highly localized on the SVE. However, because some states are observed to have support on multiple sites, they may not be localized in the strict sense, but instead may be multifractal, critical states [24,25]. Determining whether this is the case is worthy of further investigation. Here, we describe the states as *effectively localized*.

The number of effectively localized states is directly related to the number of SVEs. We empirically observe that there is one state for every X vertex [Fig. 3(a)], one for every Y [Fig. 3(b)], two for every Z [Figs. 3(c) and 3(d)], and three for every ST [Figs. 3(e) and 3(f); there are two orthogonal states that look like Fig. 3(e)]. Thus, the total number of effectively localized states n_{loc} is given by

$$n_{\mathrm{loc}} \equiv N_X + N_Y + 2N_Z + 3N_{ST}, \tag{3}$$

where $N_{\mathbf{V}}$ is the number of SVEs of type $\mathbf{V}$. For different renditions from the same LI class, the number will differ.

In the infinite-system limit, the fraction of effectively localized states for LI class γ is given by

$$\phi(\gamma) = F_X(\gamma) + F_Y(\gamma) + 2F_Z(\gamma) + 3F_{ST}(\gamma), \tag{4}$$

where $F_{\mathbf{V}}$ is the density of SVEs of type $\mathbf{V}$, shown in Fig. 4(a). We plot $\phi(\gamma)$ in Fig. 4(b). All of our numerical results thus far, which are summarized below, support the counting of effectively localized states according to Eqs. (3) and (4). The SVEs that are composed of a greater number of acute rhombi and which are more symmetric (i.e., Z and ST) have a larger number of states per SVE.

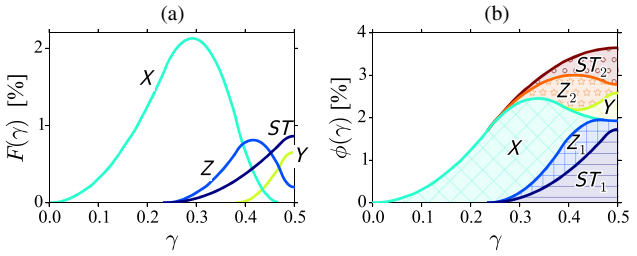

FIG. 4. (a) Density F of the four special vertex environments (shown in Fig. 2), versus LI class γ. (b) Expected fraction ϕ of special states (shown in Fig. 3) versus LI class γ.

Let ω_i^L, ω_i^H be the lower and upper frequencies of the ith band. It is useful to define, for a given tiling, the *upper-band edge frequency* ω_+ and the *lower-band edge frequency* ω_- as follows:

$$\omega_+ \equiv \omega_N^L, \qquad \omega_- \equiv \omega_{N-n_{\mathrm{loc}}}^H \tag{5}$$

where N is the number of vertices in the unit cell. Figure 5 shows ω_+, ω_-, and their average, plotted for several samples from different LI classes γ, for different degrees of approximants. Several observations can be made:

First, ω_+ and ω_- do not change significantly versus the degree of the approximant, characterized by N. This indicates that these quantities quickly converge to the values of the ideal, infinite system.

Second, ω_+ and ω_- remain approximately constant versus γ. For the Penrose LI class, the region between ω_- and ω_+ is called the *fundamental band gap*. Extending this definition to all LI classes, we find that the effectively localized states counted by Eq. (3) are high-frequency states lying within the fundamental band gap.

Finally, the fraction of these states appears to stay constant as the degree of the approximant increases. This is contrary to what we would expect if these effectively localized states arose from defects. We thus conclude that

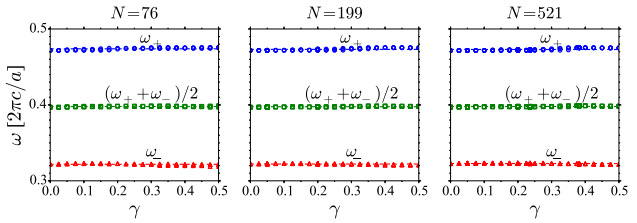

FIG. 5. Upper-band edge frequency $\omega_+ \equiv \omega_N^L$ (blue circles, top), lower-band edge frequency $\omega_- \equiv \omega_{N-n_{\mathrm{loc}}}^H$ (red triangles, bottom), and the central frequency (green squares, middle), versus γ. As discussed in the text, ω_+ and ω_- correspond to the upper and lower edges, respectively, of the fundamental band gap. Dashed lines represent the average value for a given curve. Each panel is a different degree of approximant, with increasing degree from left to right. The number of points in the unit cell is shown above each panel ($N = 76$, 199, 521).

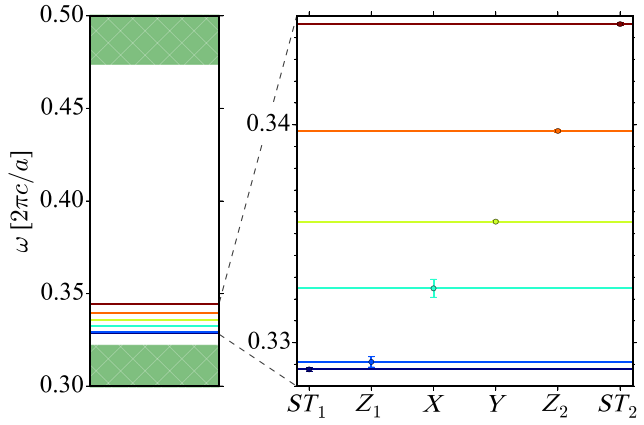

FIG. 6. The average frequencies of effectively localized states (shown in Fig. 3). In the left panel, the green, solid regions at the upper and lower ends represent the continuum of states adjacent to the fundamental band gap. The right panel, which is a blown-up portion of the left panel around the effectively localized states, identifies which effectively localized states correspond to the different frequencies.

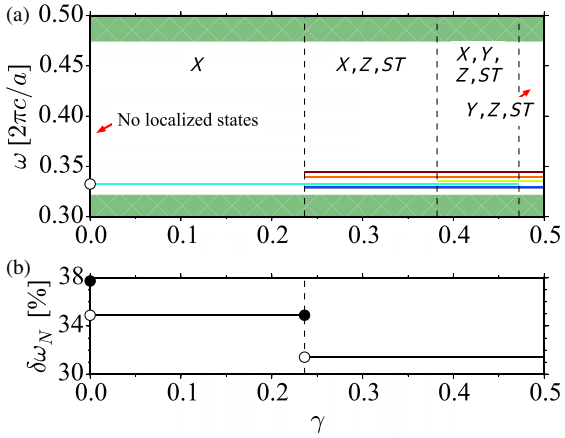

FIG. 7. (a) Expected TM spectrum around the fundamental bandgap versus LI class γ. Average frequencies of effectively localized states are shown within each range of γ that their corresponding SVEs appear. Also labeled are the SVE types occurring within each range of γ. Green, solid regions at the upper and lower ends represent the continuum of states adjacent to the band gap. Note: $\gamma = 0$ (Penrose LI class) has no SVEs and no corresponding effectively localized states. (b) Expected outer band gap versus LI class γ.

these effectively localized states are not defects, but are, rather, robust states that arise due to the SVEs.

Figure 6 shows the average midband frequency for each type of state. Within uncertainties, all states of a given type have the same frequency (i.e., are degenerate), and frequencies for different types do not overlap. This indicates that each type has a characteristic frequency.

We also observe that the characteristic frequencies do not vary significantly versus γ, which suggests that these states are primarily attributable to the presence of SVEs and not to the global structure of the tiling. This supports a hypothesis, based on the study of one unspecified LI class [26–28], that these states can be described as local resonances between closely neighboring scatterers that are arranged in highly symmetric configurations. Further evidence is that the four SVEs have the largest numbers of adjacent acute rhombi (at least four); all other vertex environments contain fewer than four adjacent acute rhombi.

From these observations, we expect that the TM spectrum around the fundamental band gap varies with γ according to Fig. 7(a). We also expect the *outer band gap*—the width of the gap between bands N and $N+1$, normalized by the midgap frequency—varies with γ according to Fig. 7(b).

We thus discover that the Penrose LI class is exceptional for being the only class with no effectively localized TM states; as a consequence, it has the largest outer band gap. All other LI classes have, generically, effectively localized TM states within the fundamental band gap with predictable and tunable degeneracies [Fig. 4(b)] and frequencies (Fig. 6) and are related to the presence of SVEs. Our initial studies using other choices of dielectric decoration show qualitatively the same results, although some choices also produce effectively localized states within the *air* component of the heterostructure.

Discussion.—Our results reveal a deep connection between the localized states and restorability. A quasicrystal pattern is restorable if it can be uniquely specified given only a set of rules that fix the allowed clusters within a circle whose radius is smaller than some bound [9]. The bound can be used to derive a lower limit on the density of configurations of any given size, including the special vertex environments (SVEs). The *restorable* LI classes [10,16] correspond to $\gamma = n\tau$ ($n \in \mathbb{Z}$), a countable subset of measure zero in the spectrum of all LI classes described by the continuous parameter γ. The localization sites occur with non-negligible density, and hence may be multifractal critical states [24,25] rather than localized in the strict sense.

By contrast, within the uncountable set of nonrestorable LI classes, γ may be varied such that the densities of some configurations can be made arbitrarily small, as illustrated in Fig. 4 for the case of SVEs. If the configuration is the site of a localized state (say, with the field falling away exponentially from the center, as suggested by the simulations for SVEs), then the state is strictly localized in the limit that the density approaches zero.

While our study is only in the case of vertex environments, the same may apply for larger configurations—that is, there may be larger clusters of obtuse and acute rhombi that are sites of localized states, and there may be sequences of LI classes for which their density approaches zero. Similar thresholds almost surely apply to LI classes obtained by extensions of the dual method that are parametrized by additional degrees of freedom aside from γ (such as lattices dual to quasiperiodic pentagrids), and it may be worth studying such examples for the purpose of

applications. We note that a similar study in 1D is not possible for the analogue Fibonacci lattice because the projection produces only one distinct LI class; however, there are other studies done on photonic localization in 1D quasiperiodic systems [29,30].

*Corresponding author.
chaneylin@gmail.com

[1] D. Levine and P. J. Steinhardt, Phys. Rev. Lett. **53**, 2477 (1984).
[2] D. Levine and P. J. Steinhardt, Phys. Rev. B **34**, 596 (1986).
[3] J. E. S. Socolar and P. J. Steinhardt, Phys. Rev. B **34**, 617 (1986).
[4] P. J. Steinhardt and D. P. DiVincenzo, *Quasicrystals: The State of the Art*, Series on Directions in Condensed Matter Physics Vol. 16, 2nd ed. (World Scientific, Singapore, 1999).
[5] H. Altug, D. Englund, and J. Vučković, Nat. Phys. **2**, 484 (2006).
[6] I. El-Kady, M. M. R. Taha, and M. F. Su, Appl. Phys. Lett. **88**, 253109 (2006).
[7] Y. S. Chan, C. T. Chan, and Z. Y. Liu, Phys. Rev. Lett. **80**, 956 (1998).
[8] Z. V. Vardeny, A. Nahata, and A. Agrawal, Nat. Photonics **7**, 177 (2013).
[9] L. S. Levitov, Commun. Math. Phys. **119**, 627 (1988).
[10] K. Ingersent and P. J. Steinhardt, Phys. Rev. Lett. **64**, 2034 (1990).
[11] R. Penrose, Bull. Inst. Math. Appl. **10**, 266 (1974).
[12] M. Gardner, Sci. Am. **236**, No. 1, 110 (1977).
[13] N. G. de Bruijn, Indagat. Math **84**, 39 (1981).
[14] N. G. de Bruijn, Indagat. Math **84**, 53 (1981).
[15] J. E. S. Socolar, P. J. Steinhardt, and D. Levine, Phys. Rev. B **32**, 5547 (1985).
[16] C. Lin, P. J. Steinhardt, and S. Torquato, J. Phys. Condens. Matter **29**, 204003 (2017).
[17] O. Entin-Wohlman, M. Kléman, and A. Pavlovitch, J. Phys. (Paris) **49**, 587 (1988).
[18] E. Zobetz and A. Preisinger, Acta Crystallogr. Sect. A **46**, 962 (1990).
[19] A. Pavlovitch and M. Kléman, J. Phys. A **20**, 687 (1987).
[20] J. D. Joannopoulos, S. G. Johnson, J. N. Winn, and R. D. Meade, *Photonic Crystals: Molding the Flow of Light* (Princeton University Press, Princeton, NJ, 2011).
[21] S. Johnson and J. Joannopoulos, Opt. Express **8**, 173 (2001).
[22] M. C. Rechtsman, H.-C. Jeong, P. M. Chaikin, S. Torquato, and P. J. Steinhardt, Phys. Rev. Lett. **101**, 073902 (2008).
[23] M. Florescu, S. Torquato, and P. J. Steinhardt, Phys. Rev. B **80**, 155112 (2009).
[24] T. Tokihiro, T. Fujiwara, and M. Arai, Phys. Rev. B **38**, 5981 (1988).
[25] P. Repetowicz, U. Grimm, and M. Schreiber, Phys. Rev. B **58**, 13482 (1998).
[26] K. Wang, Phys. Rev. B **73**, 235122 (2006).
[27] K. Wang, Phys. Rev. B **76**, 085107 (2007).
[28] K. Wang, Phys. Rev. B **82**, 045119 (2010).
[29] R. Peng, M. Wang, A. Hu, S. Jiang, G. Jin, and D. Feng, Phys. Rev. B **57**, 1544 (1998).
[30] R. Peng, Y. Liu, X. Huang, F. Qiu, M. Wang, A. Hu, S. Jiang, D. Feng, L. Ouyang, and J. Zou, Phys. Rev. B **69**, 165109 (2004).